Table 2. The list of genes which changed significantly in P14SC

ID	Symbol	Entrez Gene name	Type(s)
Increase			
1386904_a_at	CYB5A	cytochrome b5 type A (microsomal)	enzyme
1387897_at	CNP	2',3'-cyclic nucleotide 3' phosphodiesterase	enzyme
1370048_at	LPAR1	lysophosphatidic acid receptor 1	G-protein coupled receptor
1368092_at	FAH	fumarylacetoacetate hydrolase (fumarylacetoacetase)	enzyme
1368506_at	RGS4	regulator of G-protein signaling 4	other
1368298_at	ADCY5	adenylate cyclase 5	enzyme
1370834_at	HS3ST1	heparan sulfate (glucosamine) 3-O-sulfotransferase 1	enzyme
1368154_at	GUCY1A3	guanylate cyclase 1, soluble, alpha 3	enzyme
1368145_at	PCP4	Purkinje cell protein 4	other
1368253_at	GAMT	guanidinoacetate N-methyltransferase	enzyme
1387822_at	GNA11	guanine nucleotide binding protein (G protein), alpha 11 (Gq class)	enzyme
1368263_a_at	MOBP	myelin-associated oligodendrocyte basic protein	other
1367949_at	PENK	proenkephalin	other
1370206_at	ACCN4	amiloride-sensitive cation channel 4, pituitary	ion channel
1386979_at	SERINC5	serine incorporator 5	transporter
1368104_at	TSPAN2	tetraspanin 2	other
1372462_at	ACAT2	acetyl-CoA acetyltransferase 2	enzyme
1398257_at	MOG	myelin oligodendrocyte glycoprotein	other
1398258_at	APOD	apolipoprotein D	transporter
1368105_at	TSPAN2	tetraspanin 2	other
1368384_at	KLK6	kallikrein-related peptidase 6	peptidase
1370541_at	NR1D2	nuclear receptor subfamily 1, group D, member 2	ligand-dependent nuclear receptor
1370693_a_at	CNP	2',3'-cyclic nucleotide 3' phosphodiesterase	enzyme
1368121_at	AKR7A3	aldo-keto reductase family 7, member A3 (aflatoxin aldehyde reductase)	enzyme
1368438_at	PDE10A	phosphodiesterase 10A	enzyme
1368858_at	UGT8	UDP glycosyltransferase 8	enzyme
1370372_at	RASD2	RASD family, member 2	enzyme
1370816_at	NR1D1	nuclear receptor subfamily 1, group D, member 1	ligand-dependent nuclear receptor
1368478_at	DRD1	dopamine receptor D1	G-protein coupled receptor
1370669_a_at	PDE10A	phosphodiesterase 10A	enzyme
1387874_at	DBP	D site of albumin promoter (albumin D-box) binding protein	transcription regulator
1388176_at	Cml5	camello-like 5	enzyme
1368135_at	NINJ2	*ninjurin* 2	other
1368127_at	NEU2	sialidase 2 (cytosolic sialidase)	enzyme
1368479_at	DRD1	dopamine receptor D1	G-protein coupled receptor

Table 2. (Continued)

ID	Symbol	Entrez Gene name	Type(s)
Increase			
1387241_at	GPR88	G protein-coupled receptor 88	G-protein coupled receptor
1368708_a_at	DRD2	dopamine receptor D2	G-protein coupled receptor
1368300_at	ADPRA2A	adenosine A2a receptor	G-protein coupled receptor
1368500_a_at	RGS9	regulator of G-protein signaling 9	enzyme
1370991_at	Cml3/Gm4477	camello-like 3	enzyme
Decrease			
1370550_at	LSAMP	limbic system-associated membrane protein	other
1370026_at	CRYAB	crystallin, alpha B	other
1386987_at	IL6R	interleukin 6 receptor	transmembrane receptor
1368641_at	WNT4	wingless-like MMTV integration site family, member 4	cytokine
1387169_at	TLE3	transducin-like enhancer of split 3 (E(sp 1) homolog, Drosophila)	other
1368577_at	GJB6	gap junction protein, beta 6, 30kDa	transporter
1386929_at	HK1	hexokinase 1	kinase
1368782_at	SSTR2	somatostatin receptor 2	G-proein coupled receptor
1368677_at	BDNF	brain-derived neurotrophic factor	growth factor
1387908_at	RASD1	RAS, dexamethasone-induced 1	enzyme
1370019_at	SULT1A1	sulfotransferase family, cytosolic, 1A, phenol-preferring, member 1	enzyme
1398245_at	SNCG	synuclein, gamma (breast cancer-specific protein 1)	other
1388271_at	MT2A	metallothionein 2A	other

ID, symbol, entrez gene name, type of each gene were shown based on IPA software database.

Table 3. The list of genes which changed significantly in E12IP and P14SC were categorized to groups based on their functions using IPA software

E12IP			P14SC	
p-value	Molecules	Category	P14SC	p-value
		Behavior	RGS9,GJB6,RASD2,DBP,BDNF,PDE10A,IL6R,CNP,SNCG,DRD2,PCP4,DRD1,NR1D1,LPAR1,ADCY5,PENK,ADORA2A	2.16E-07-1.85E-02
1.02E-02-1.02E-02	RHOA	Cell Cycle	CRYAB,SSTR2,WNT4	4.65E-03-1.85E-02
6.33E-06-3.04E-02	ABCB1,CD59,MT2A,RHOA,ACTB,GREM1,VDAC1,MT1E	Cell Death	CRYAB,BDNF,IL6R,RGS4,UGT8,DRD2,HK1,LPAR1,SSTR2,ADCY5,MT2A,ADORA2A,MOG	3.03E-04-2.31E-02
2.56E-03-4.46E-02	CD59,HBB,MT2A,RHOA,SLC1A3,VDAC1	Cell Morphology	HK1,LPAR1,DRD1,MT2A,BDNF,IL6R,GNA11,KLK6,RGS4,SNCG,DRD2,ADORA2A	4.59E-04-2.31E-02
4.93E-02-4.93E-02	CD59,HBA1/HBA2,VDAC1	Cell Signaling	RGS9,LPAR1,SSTR2,DRD1,BDNF,ADCY5,PDE10A,IL6R,GNA11,RGS4,DRD2,ADORA2A	9.12E-05-2.07E-02
6.3E-05-2.54E-02	CD59,MT2A,RHOA,SLC1A3,GREM1,GABARAP,VDAC1,LPHN1,MT1E,S100A10	Cell-To-Cell Signaling and Interaction	RASD2,GUCY1A3,BDNF,GNA11,CNP,IL6R,RGS4,KLK6,SNCG,DRD2,PCP4,DRD1,ADCY5,MT2A,SULT1A1,PENK,ADORA2A,MOG,NINJ2	2.34E-07-2.31E-02
6.33E-06-4.27E-02	SYNJ2,CD59,MT2A,RHOA,HBA1/HBA2,VDAC1,LPHN1,MT1E	Cellular Assembly and Organization	RGS9,HK1,CRYAB,LPAR1,DRD1,MT2A,BDNF,GNA11,CNP,SNCG,DRD2,MOG	4.65E-03-2.31E-02
4.67E-04-4.46E-02	Tsc22d3,HBB,MT2A,RHOA,HBA1/HBA2,SLC1A3,	Cellular Development	NR1D1,DRD1,MT2A,BDNF,SERINC5,IL6R,RGS4,UGT8,DRD2	5.55E-04-2.31E-02
1.32E-04-4.27E-02	CD59,MT2A,RHOA,HBA1/HBA2,VDAC1,LPHN1,MT1E	Cellular Function and Maintenance	CRYAB,DRD1,BDNF,CNP	4.65E-03-2.31E-02
4.67E-04-2.07E-02	ABCB1,MT2A,RHOA,ACTB,GREM1,GABARAP,VDAC1,MT1E	Cellular Growth and Proliferation	GJB6,CRYAB,GUCY1A3,BDNF,IL6R,GNA11,KLK6,RGS4,SNCG,DRD2,RASD1,SSTR2,LPAR1,NR1D1,MT2A,PENK,WNT4,ADORA2A,MOG	3.03E-04-2.17E-02
2.56E-03-4.77E-02	CD59,RHOA,LPHN1,S100A10	Cellular Movement	GUCY1A3,BDNF,GNA11,CNP,IL6R,RGS4,KLK6,SNCG,DRD2,NR1D1,SSTR2,DRD1,LPAR1,PENK,ADORA2A,MOG	6.76E-05-1.85E-02
1.67E-05-2.54E-02	Tsc22d3,MT2A,RHOA,GREM1,VDAC1,MT1E	Connective Tissue Development and Function		
5.12E-03-4.27E-02	HBB,RHOA,PNLIP	Developmental Disorder	CRYAB,GJB6,SSTR2,DRD1,GUCY1A3,BDNF,IL6R,GNA11,WNT4,RGS4,DRD2	2.02E-05-2.31E-02
7.67E-03-7.67E-03	ABCB1	DNA Replication, Recombination, and Repair	GUCY1A3,BDNF,RGS4,DRD2,ADORA2A	1.28E-02-1.28E-02
2.56E-03-4.27E-02	ABCB1	Drug Metabolism	DRD1,BDNF,SULT1A1,GNA11,RGS4,SNCG,DRD2,ADORA2A	2.12E-05-1.85E-02
2.56E-03-4.77E-02	HBB,RHOA,GREM1	Embryonic Development	GJB6,LPAR1,BDNF,WNT4,KLK6,DRD2	1.17E-03-1.85E-02
2.56E-03-2.56E-03	ABCB1	Endocrine System Development and Function	BDNF,SULT1A1,GNA11,WNT4,ADORA2A	2.1E-04-2.31E-02
2.25E-02-2.25E-02	MT1E,S100A10	Endocrine System Disorders	ACAT2,SSTR2,DRD1,IL6R,DRD2	2.02E-05-2.31E-02
4.52E-02-4.52E-02	RHOA	Gene Expression	DBP,BDNF,IL6R,RGS4,KLK6,NR1D2,DRD2,RASD1,NR1D1,DRD1,LPAR1,TLE3,WNT4,ADORA2A,MOG	1.38E-02-1.39E-02

Table 3. (Continued)

E12IP			P14SC	
p-value	Molecules	Category	P14SC	p-value
1.29E-03-4.27E-02	ABCB1,HBB,MT2A,ACTB,PNLIP,MT1E	Genetic Disorder	ACCN4,RGS9,CRYAB,GJB6,RASD2,ACAT2,BDNF,GNA11,KLK6,NR1D2,DRD1,ADCY5,MT2A,WNT4,LSAMP,MOG,GUCY1A3,DBP,PDE10A,CNP,IL6R,TSPAN2,RGS4,NEU2,SNCG,DRD2,GPR88,FAH,PCP4,LPAR1,NR1D1,MOBP,SSTR2,SULT1A1,PENK,TLE3,CYB5A,ADORA2A,APOD	4.1E-09-2.31E-02
2.56E-03-4.27E-02	ABCB1,RHOA,MT1E	Inflammatory Disease	CRYAB,BDNF,IL6R,DRD2,MOG	4.65E-03-2.31E-02
2.56E-03-4.27E-02	CD59,RHOA,MT1E,S100A10	Inflammatory Response	GNA11,IL6R,PENK,CNP,ADORA2A,MOG	9.29E-03-2.31E-02
2.56E-03-4.4E-02	SYNJ2,ABCB1,MT2A,DLAT,RHOA,MT1E,PNLIP,S100A10	Lipid Metabolism	ACAT2,DBP,BDNF,SERINC5,GNA11,RGS4,UGT8,DRD2,LPAR1,DRD1,SSTR2,SULT1A1,WNT4,ADORA2A,MOG,APOD	2.1E-04-2.31E-02
6.33E-06-4.93E-02	ABCB1,CD59,HBA1/HBA2,CDK16,SLC1A3,HEPH,LPHN1,HBB,MT-CYB,MT2A,RHOA,GABARAP,VDAC1,MT1E,PNLIP,S100A10	Molecular Transport	ACAT2,GUCY1A3,BDNF,PDE10A,GNA11,IL6R,RGS4,UGT8,SNCG,DRD2,HK1,LPAR1,SSTR2,DRD1,MT2A,ADCY5,WNT4,ADORA2A,APOD	1.11E-05-2.31E-02
3.99E-03-4.27E-02	MT2A,RHOA,HBA1/HBA2,SLC1A3,GABARAP,VDAC1,LPHN1,MT1E	Nervous System Development and Function	GJB6,RASD2,GUCY1A3,DBP,BDNF,SERINC5,CNP,GNA11,RGS4,UGT8,SNCG,DRD2,PCP4,DRD1,NR1D1,LPAR1,ADCY5,MT2A,PENK,ADORA2A,MOG,NINJ2	1.59E-05-2.31E-02
3.79E-05-3.78E-02	MT2A,ACTB,SLC1A3,MT1E,S100A10	Neurological Disease	RGS9,CRYAB,RASD2,GJB6,BDNF,GNA11,DRD1,MT2A,ADCY5,LSAMP,MOG,GUCY1A3,DBP,PDE10A,CNP,IL6R,RGS4,SNCG,DRD2,GPR88,PCP4,LPAR1,MOBP,SSTR2,NR1D1,PENK,ADORA2A,APOD	1.43E-09-2.31E-02
2.64E-02-2.64E-02	MT2A,MT1E	Psychological Disorders	CRYAB,BDNF,PDE10A,CNP,RGS4,DRD2,PCP4,MOBP,DRD1,SSTR2,MT2A,LSAMP,ADORA2A,MOG,APOD	1.57E-04-2.01E-02
6.33E-06-4.4E-02	ABCB1,AZIN1,HBA1/HBA2,SLC1A3,SYNJ2,HBB,MT2A,RHOA,DLAT,VDAC1,PNLIP,MT1E,S100A10	Small Molecule Biochemistry	RGS9,ACAT2,BDNF,SERINC5,GNA11,HK1,DRD1,MT2A,ADCY5,WNT4,MOG,DBP,GUCY1A3,PDE10A,IL6R,RGS4,UGT8,SNCG,DRD2,SSTR2,LPAR1,GAMT,SULT1A1,CYB5A,ADORA2A,APOD	1.11E-05-2.31E-02
2.56E-03-2.79E-02	CD59,Tsc22d3,HBB,RHOA,SLC1A3,GREM1	Tissue Development	GJB6,CRYAB,GUCY1A3,BDNF,GNA11,CNP,IL6R,KLK6,RGS4,DRD2,GAMT,DRD1,LPAR1,TLE3,WNT4,ADORA2A,MOG,NINJ2	4.59E-04-2.31E-02
3.43E-04-2.79E-02	CD59,HBB,MT2A,RHOA,SLC1A3,GREM1,MT1E,S100A10	Tissue Morphology	CRYAB,ACAT2,GUCY1A3,BDNF,IL6R,DRD2,GAMT,DRD1,SSTR2,LPAR1,WNT4,ADORA2A,MOG	8E-04-2.31E-02

Behavior'-related genes were identified only in P14SC. Additionally a larger number of genes were categorized to 'nervous system development and function', 'neurological disease', and 'psychological disorders' in P14SC than in E12IP.

ACKNOWLEDGMENT

This work was supported by Grants-in-Aid from the Food Safety Commission of Japan (No. 1003).

REFERENCES

Blackford, J.U. and Pine, D.S. (2012): Neural substrates of childhood anxiety disorders: a review of neuroimaging findings. Child Adolesc. Psychiatr. Clin. N. Am., **21**, 501-525.

Etkin, A. and Wager, T.D. (2007): Functional neuroimaging of anxiety: a meta-analysis of emotional processing in PTSD, social anxiety disorder, and specific phobia. Am. J. Psychiatry., **164**, 1476-1488.

Markram, K., Rinaldi, T., Mendola, D.L., Sandi, C. and Markram, H. (2008): Abnormal fear conditioning and amygdala processing in an animal model of autism. Neuropsychopharmacology, **33**, 901-912.

Neuhaus, E., Beauchaine, T.P. and Bernier, R. (2010): Neurobiological correlates of social functioning in autism. Clin. Psychol. Rev., **30**, 733-748.

Schneider, T. and Przewtocki, R. (2005): Behavioral alterations in rats prenatally exposed to valproic acid: Animal model of autism. Neuropsychopharmacology, **30**, 80-89.

Schneider, T., Ziolkowska, T., Gieryk, T., Tyminska, T. and Przewlocki, R. (2007): Prenatal exposure to valproic acid disturbs the enkephalinergic system functioning, basal hedonic tone, and emotional responses in an animal model of autism. Psychopharmacology, **193**, 547-555.

Schneider, T., Roman, A., Basta-Kaim, A., Kubera, M., Budziszewska, B., Schneider, K. and Przewtochi, R. (2008): Gender-specific behavioral and immunological alterations in an animal model of autism induced by prenatal exposure to valproic acid. Psychoneuroendocrinology, **33**, 728-740.

Wagner, G.C., Reuhl, K.R., Cheh, M., McRae, P. and Halladay, A.K. (2006): A new neurobehavioral model of autism in mice: Pre- and postnatal exposure to sodium valproate. J Autism Dev. Disord., **36**, 779-793.

Yochum, C.L., Dowling, P., Reuhl, K.R., Wagner, G.C. and Ming, X. (2008): VPA-induced apoptosis and behavioral deficits in neonatal mice. Brain Res., **1203**, 126-132.

Yochum, C.L., Bhattacharya, P., Patti, L., Mirochnitchenko, L. and Wagner, G.C. (2010): Animal model of autism using GSTM1 knockout mice and early post-natal sodium valproate treatment. Behav. Brain Res., **210**, 202-210.

Niflumic Acid Activates Additional Currents of the Human Glial L-Glutamate Transporter EAAT1 in a Substrate-Dependent Manner

Kanako Takahashi,[a] Reiko Ishii-Nozawa,[b] Koichi Takeuchi,[b] Ken Nakazawa,[a] Yuko Sekino,[a] and Kaoru Sato*,[a]

[a] *Laboratory of Neuropharmacology, Division of Pharmacology, National Institute of Health Sciences; 1–18–1 Kamiyoga, Setagaya, Tokyo 158–8501, Japan: and* [b] *Department of Clinical Pharmacology, Meiji Pharmaceutical University; 2–522–1 Noshio, Kiyose, Tokyo 204–8588, Japan.*
Received September 6, 2013; accepted September 29, 2013

The astrocytic L-glutamate (L-Glu) transporter EAAT1 participates in the removal of L-Glu from the synaptic cleft and maintenance of non-toxic concentrations in the extracellular fluid. We have shown that niflumic acid (NFA), a non-steroidal anti-inflammatory drug (NSAIDs), alters L-Glu-induced EAAT1 currents in a voltage-dependent manner using the two-electrode voltage clamp technique in *Xenopus* oocytes expressing EAAT1. In this study, we characterised the effects of NFA on each type of ion-flux through EAAT1. NFA modulated currents induced by both L-Glu and L-aspartate (L-Asp) in a voltage-dependent manner. Ion-substitution experiments revealed that the activation of additional H^+ conductance was involved in the modulation of currents induced by L-Asp and L-Glu, but Cl^- was involved only with the L-Asp currents. NFA activated additional currents of EAAT1 in a substrate-dependent manner.

Key words astrocytic L-glutamate transporter; niflumic acid; additional conductance; EAAT1; voltage-dependent manner

Neuronal and astrocytic L-glutamate (L-Glu) transporters (EAATs) are the only significant machinery for the removal of L-Glu from the synaptic cleft and maintenance of non-toxic concentrations in the extracellular fluid.[1] Along with controlling extracellular L-Glu concentrations, EAATs also play a role in the regulation of functional crosstalk between neurons and glial cells by modulating the ion flux. L-Glu is co-transported into a cell with 3 Na^+ and 1 H^+ by EAATs, followed by the counter-transport of 1 K^+ [2]. L-Glu and Na^+ binding to EAATs activates a non-stoichiometrically-coupled (uncoupled) Cl^- conductance.[3] The Na^+ influx triggers functional metabolic crosstalk between neurons and astrocytes,[4] and the uncoupled Cl^- conductance dampens neuronal excitability.[5,6]

Niflumic acid [2-((3-(trifluoromethyl)phenyl)amino)-3-pyridinecarboxylic acid, NFA], a member of a class of non-steroidal anti-inflammatory drugs (NSAIDs), modulates the gating of Cl^- channels,[7,8] K^+ channels,[9–14] nicotinic acetylcholine channels,[15] and transient receptor potential channels.[16] NFA also enhances the substrate-gated currents of EAAT4, an L-Glu transporter expressed primarily in Purkinje neurons,[17] by activating additional uncoupled H^+ and Cl^- conductances.[18] We recently discovered that NFA modulates the current mediated through EAAT1, an astrocytic L-Glu transporter,[19,20] in a voltage-dependent manner.[21] In this study, we characterised the effects of NFA on L-Glu and L-aspartate (L-Asp) currents, focusing on each ion-flux. We report here that the activation of additional H^+ conductance was involved in the modulation by NFA of both L-Glu currents and L-Asp currents, whereas Cl^- was involved only in the modulation of L-Asp currents.

MATERIALS AND METHODS

Expression of EAAT1 in *Xenopus* Oocytes All of the animals were treated in accordance with the guidelines for the Care and Use of Laboratory Animals of the Animal Research Committee of the National Institute of Health Sciences, Japan. A pcDNA3.1 plasmid containing the cDNA of the human glutamate transporter EAAT1 was obtained from Dr. Keiko Shimamoto (Suntory Institute for Bioorganic Research, Osaka, Japan). The plasmids containing the EAAT1 cDNA were linearized at a *Not*I (Toyobo, Osaka, Japan) site, and capped RNA was transcribed from the linearized cDNA construct with a bacteriophage T7 RNA polymerase (mMESSAGE mMACHINE; Ambion, Austin, TX, U.S.A.). Oocytes were collected from anaesthetised *Xenopus laevis*. The isolated oocytes were then treated with collagenase (2 mg mL^{-1}, type 1, Sigma, St. Louis, MO, U.S.A.), and capped mRNA was injected into either defolliculated stage V or VI oocytes. The oocytes were incubated for 2–7 d at 18°C in ND96 solution containing 96 mM NaCl, 2 mM KCl, 1.8 mM $CaCl_2$, 1 mM $MgCl_2$, and 5 mM *N*-(2-hydroxyethyl)piperazine-*N'*-(2-ethanesulfonic acid) (HEPES) (pH 7.5) supplemented with 0.01% gentamycin.

Electrophysiology Two-electrode voltage clamp recordings from EAAT1-expressing oocytes were performed at room temperature (25–27°C) using glass microelectrodes filled with 3 M KCl solution (resistance=1–4 MΩ) and an Ag/AgCl pellet bath ground (EP2; World Precision Instruments, Sarasota, FL, U.S.A.). A bath-clamp amplifier (OC-725C; Warner Instruments, Hamden, CT, U.S.A.) was used with a Digidata 1320A interface (Axon Instruments, Foster City, CA, U.S.A.). The pClamp suite of programs (ver. 8.2; Axon Instruments) and the Clampfit data acquisition software were used to control stimulation parameters, and to acquire and analyse data. An Ag/AgCl pellets were used to avoid voltage errors associated with buffer changes. Oocytes were continuously superfused with ND96 solution. To adjust the extracellular H^+ to various concentrations, the HEPES was replaced by either 2-(*N*-morpholino)ethanesulfonic acid (MES) (pH 5.5, 6.5) or [(2-hydroxy-1,1-bis(hydroxymethyl)ethyl)amino]-1-propanesulfonic acid (TAPS) (pH 8.5). For Na^+ substitution experiments, Na^+ was replaced by equimolar choline ions. For

The authors declare no conflict of interest.

*To whom correspondence should be addressed. e-mail: kasato@nihs.go.jp

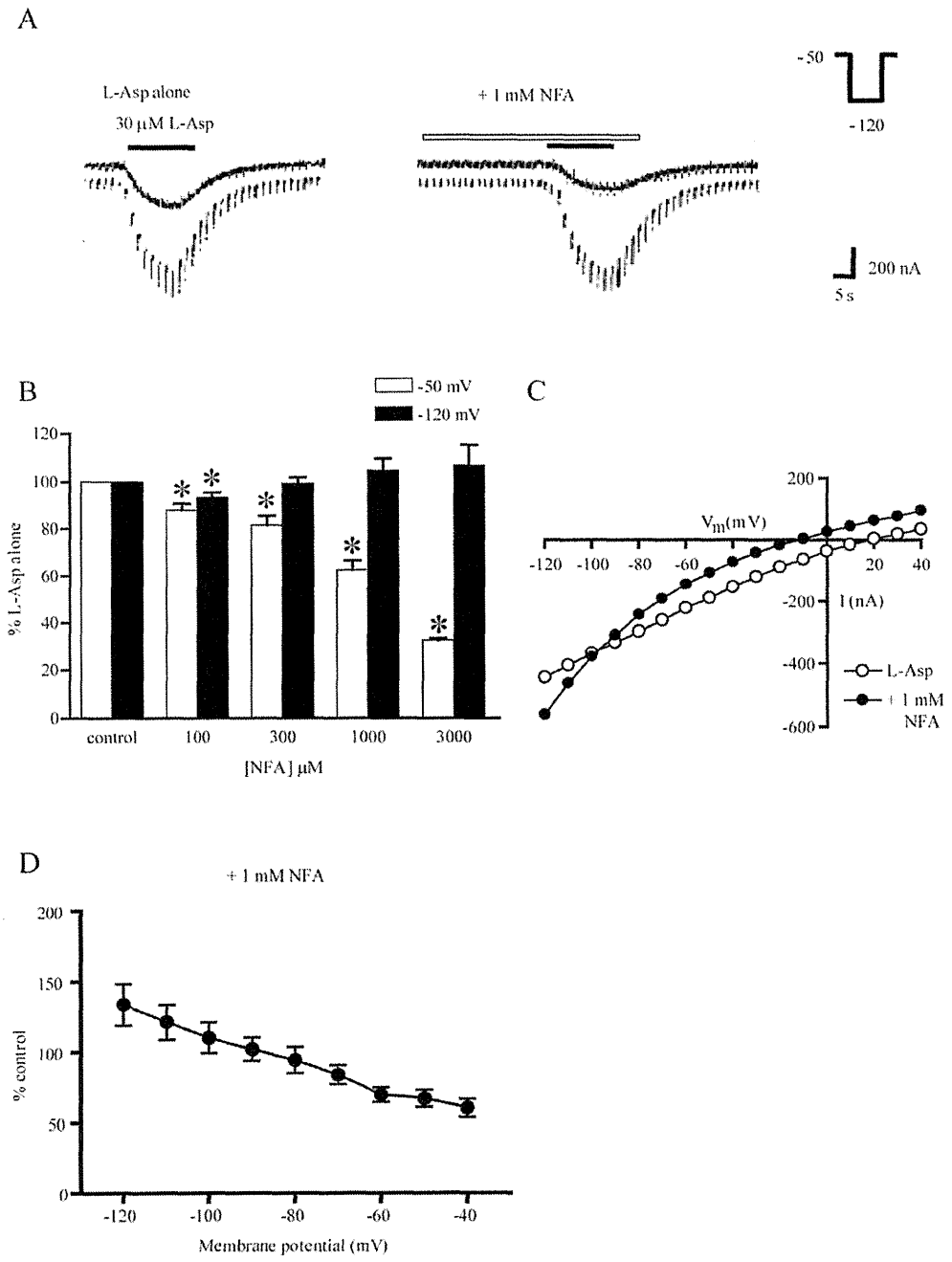

Fig. 1. Niflumic Acid (NFA) Modulated L-Asp-Induced Currents in *Xenopus* Oocytes Expressing EAAT1 in a Voltage-Dependent Manner

A: The traces of L-Asp (30 μM)-induced inward currents in either the absence or presence of NFA (1 mM) at −50 mV (bold line) and −120 mV (thin line). The oocytes were held at −50 mV and hyperpolarised to −120 mV for 400 ms every 2 s. B: Concentration–response relationships of the effects of NFA on L-Asp currents at −50 mV and −120 mV. The effects of NFA on the peak amplitude of the L-Asp current were examined by comparing the current in the presence of NFA to that recorded just prior to the drug treatment (control response) at each concentration. Data are analysed by paired *t*-test. Graph shows the summary of the results. Each column shows the averaged data normalized to the control (4–5 oocytes for each) at each concentration. At −50 mV, NFA inhibited the peak amplitudes of the L-Asp currents in a concentration-dependent manner, whereas NFA only slightly increased the peak amplitude of the L-Asp-induced currents at −120 mV. *$p<0.05$ *vs.* control. C: Representative current–voltage relationships for L-Asp (30 μM) in either the absence or presence of NFA (1 mM). The current–voltage relationships were obtained with a holding potential of −50 mV and implementation of 400-ms voltage jumps in 10 mV increments over the range from −120 mV to +40 mV. For the control, the current values at steady state were subtracted from those measured in the presence of L-Asp. For the NFA-treated group, the current values in the presence of NFA alone were subtracted from those in the presence of both NFA and L-Asp. NFA treatment produced a leftward shift of E_{rev} (from 18.4±5.4 to −2.7±4.1 mV; $n=10$, $p<0.05$, paired *t*-test). D: The relationship between the effects and the holding potential. The current in the presence of NFA was normalized to that obtained just before the application of NFA. The effects of NFA was voltage-dependent ($n=10$).

the Cl^- substitution experiments, Cl^- was replaced by equimolar gluconate ions. Oocytes were bathed in an experimental chamber (0.5 mL) filled with ND96 solution and voltage-clamped at −50 mV. A 400 ms hyperpolarising voltage step to −120 mV was applied every 2 s to confirm clamp conditions and observe the voltage dependence of current responses. As

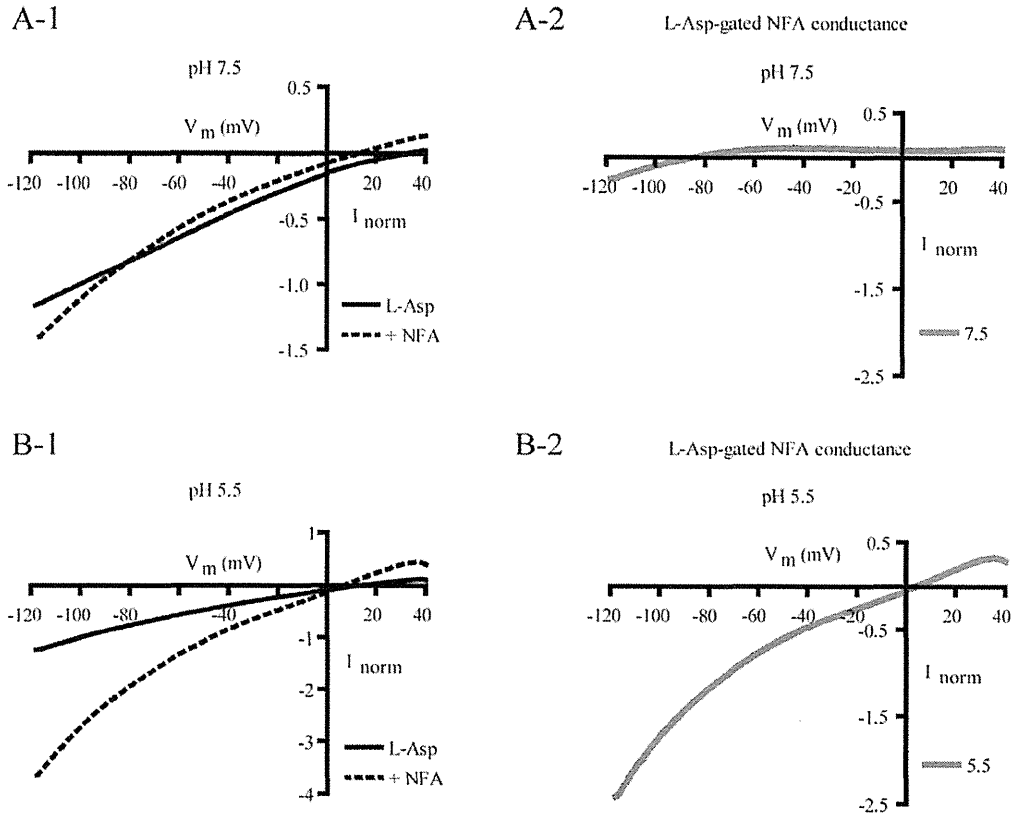

Fig. 2. Influence of Extracellular pH on L-Asp Currents in Either the Absence or Presence of NFA

The current–voltage relationships were determined using a holding potential of −50 mV and implementing an 800 ms ramp pulse over the range from +40 mV to −120 mV. The current–voltage relationships for the L-Asp-gated NFA-induced conductance were obtained by subtracting the control L-Asp currents from the L-Asp currents in the presence of NFA. The currents are normalised to the amplitude of the L-Asp currents generated at −100 mV. A-1 and B-1: Average current–voltage relationships for L-Asp (30 μM) in either the absence (solid line) or presence (dotted line) of NFA (300 μM) at pH 7.5 (A-1) and pH 5.5 (B-1). A-2 and B-2: Average current–voltage relationships for the L-Asp-gated NFA-induced conductance at pH 7.5 (A-2) and pH 5.5 (B-2). The average shift of the sub-E_{rev} was −45.1±4.0 mV per pH unit, which is consistent with that reported for H^+-selective channels. Each point represents the mean value from 5 oocytes.

a substrate, 30 μM of either L-Glu or L-Asp (half of the EC_{50}) was applied to the oocytes by superfusion at 0.2 mL·s^{-1} of constant flow rate for 15 s with regular 30 s intervals. NFA was applied from 30 s before to 5 s after the end of the application of substrate. The current–voltage relationships for substrate transport were determined by subtracting the steady-state currents obtained with a holding potential of −50 mV either implementing 400 ms voltage jumps in 10 mV increments from −120 to +60 mV or implementing an 800 ms ramp pulse from −120 to +40 mV in the absence of substrate from the corresponding currents in the presence of substrate. The currents are normalised to the amplitude of the L-Asp or L-Glu currents generated at −100 mV (Figs. 2–8).

Preparation of the Compounds All chemicals were purchased from Wako (Tokyo, Japan) unless otherwise stated. NFA, TAPS, and MES were purchased from Sigma (St. Louis, MO, U.S.A.). L-Asp and L-Glu stock solutions (20 mM) were made in purified water (Millipore, Billerica, MA, U.S.A.). The NFA stock solution (300 mM) was made in dimethyl sulfoxide (DMSO) and dissolved in ND96 solution immediately prior to each experiment. The pH of every solution was adjusted to 7.5, and the final concentrations of the solvents were less than 1%.

Statistical Analysis All of the data are presented as the mean±S.E.M. p Values were obtained by statistical analysis, as noted in the figure legends.

RESULTS

Effects of NFA on L-Asp-Induced Currents in *Xenopus* Oocytes Expressing EAAT1 We first examined the effects of NFA on the L-Asp-induced currents in *Xenopus* oocytes expressing EAAT1. The left trace in Fig. 1A represents the inward control current produced by L-Asp (30 μM) voltage clamped at −50 mV with 400 ms hyperpolarising voltage steps to −120 mV every 2 s. At −50 mV, NFA (300 μM–3 mM) inhibited the peak amplitude of the L-Asp-induced currents in a concentration-dependent manner, whereas at 120 mV, NFA only slightly increased the peak amplitude of the L-Asp-induced currents (Figs. 1A, B). Figure 1C shows the representative current–voltage relationships for L-Asp (30 μM)-induced currents in either the presence or absence of 1 mM NFA. In the absence of NFA, the L-Asp current was linear in a voltage-dependent manner, with the reversal potential (E_{rev}) at 18.4±5.4 mV. NFA treatment resulted in a leftward shift of the E_{rev} of the L-Asp currents (from 18.4±5.4 to −2.7±4.1 mV; n=10, p<0.05, paired t-test). The current–voltage curve recorded in the presence of NFA crossed the control curve at

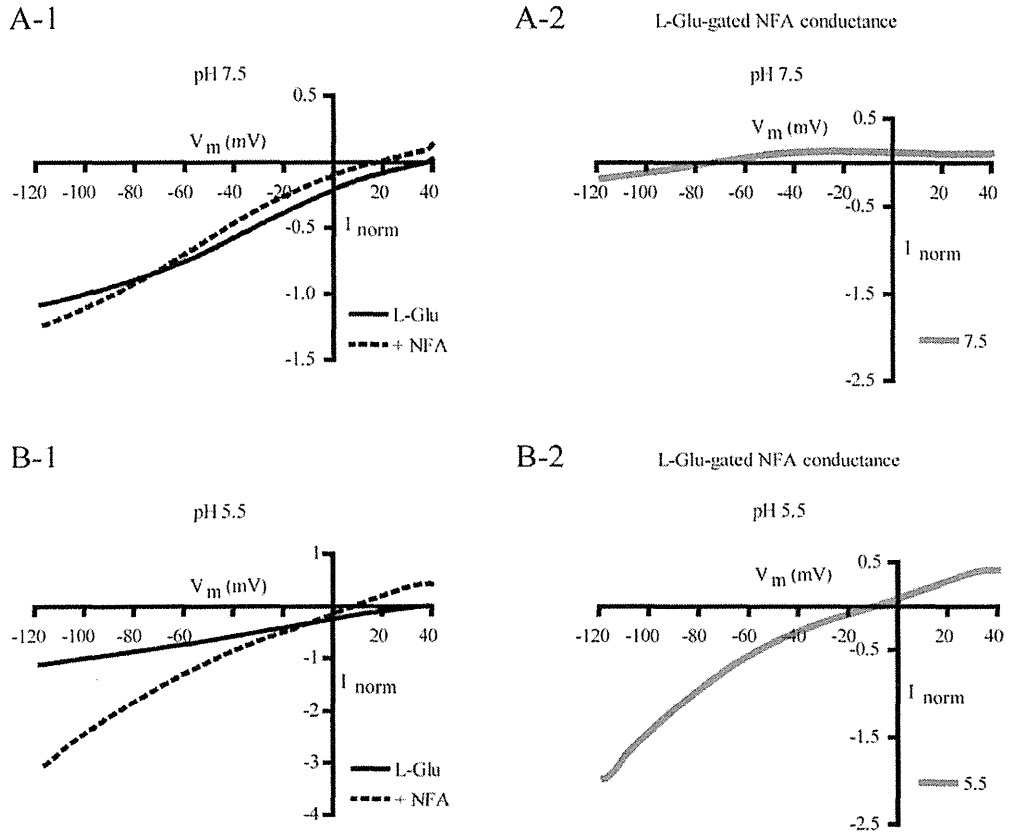

Fig. 3. Influence of Extracellular pH on L-Glu Currents in Either the Absence or Presence of NFA

A-1 and B-1: Average current–voltage relationships for L-Glu (30 μM) in either the absence (solid line) or presence (dotted line) of NFA (300 μM) at pH 7.5 (A-1) and pH 5.5 (B-1). A-2 and B-2: Average current–voltage relationships for the L-Glu-gated NFA-induced conductance at pH 7.5 (A-2) and pH 5.5 (B-2). The average shift of the sub-E_{rev} was −36.6±4.6 mV per pH unit, which is consistent with that reported for H^+-selective channels. Each point represents the mean value from 5 oocytes.

−96.5 mV (cross-over potential), indicating that NFA inhibited the L-Asp currents at potentials more positive than −96.5 mV and increased the currents at potentials more negative than −96.5 mV. The influence of NFA on the peak current amplitude was voltage-dependent (Fig. 1D). This voltage-dependent effect of NFA has also been observed with L-Glu current in our previous study.[21]

Involvement of Additional H^+ Conductance We examined whether any additional H^+ conductance is involved in these voltage-dependent effect of NFA. The effects of NFA were examined when the extracellular pH was 7.5 and 5.5. Figures 2A-1 and B-1 show the average current–voltage relationships for the L-Asp current (30 μM) in either the absence (solid line) or presence (dotted line) of NFA (300 μM) at pH 7.5 (Fig. 2A-1) and pH 5.5 (Fig. 2B-1). At pH 7.5, the curve of the L-Asp current in the presence of NFA crossed the control curve at −84 mV, whereas the crossover potential was at +4 mV at pH 5.5. The L-Asp-gated NFA-induced conductance was obtained by subtracting the L-Asp current from the L-Asp current in the presence of NFA (Figs. 2A-2, B-2). As the extracellular H^+ concentration increased, the E_{rev} of the L-Asp-gated NFA-induced conductance (sub-E_{rev}) shifted toward the more positive membrane potential. The average shift of the sub-E_{rev} gated by L-Asp was −45.1±4.0 mV per pH unit (n=5), which is consistent with previous reports for H^+-selective channels,[22,23] suggesting that NFA promotes additional H^+ conductance. Regarding L-Glu currents (Fig. 3), as the extracellular H^+ concentrations increased, the crossover potential shifted toward the more positive potential (Figs. 3A-1, B-1), and the sub-E_{rev} also shifted toward a more positive membrane potential (Figs. 3A-2, B-2). The average shift of the sub-E_{rev} gated by L-Glu changed −36.6±4.6 mV per pH unit (n=5), suggesting that NFA promotes additional H^+ conductance in this case as well. There were no significant differences between the average shifts of the sub-E_{rev} per pH unit gated by L-Asp and L-Glu (Student's t-test, p=0.2).

Involvement of Additional Na^+ Conductance We examined if the additional Na^+ conductance is involved in these voltage-dependent effect of NFA. The current–voltage relationships for the L-Asp current in either the absence or presence of NFA were examined under various extracellular [Na^+] by choline substitution. Figures 4A-1 and B-1 show the average current–voltage relationships for L-Asp in either the absence (solid line) or presence (dotted line) of NFA (300 μM) at normal [Na^+] (96 mM) (Fig. 4A-1) and low [Na^+] (24 mM) (Fig. 4B-1). Decreasing the extracellular [Na^+] resulted in a loss of crossover between −120 mV and +40 mV, indicating that low extracellular [Na^+] results in a loss of the voltage-dependent modulation of L-Asp currents by NFA. The L-Asp-gated NFA-induced conductance-voltage relationships displayed inward rectification with the sub-E_{rev} at −58 mV (Fig. 4A-2) at normal [Na^+], whereas no significant subtracted currents

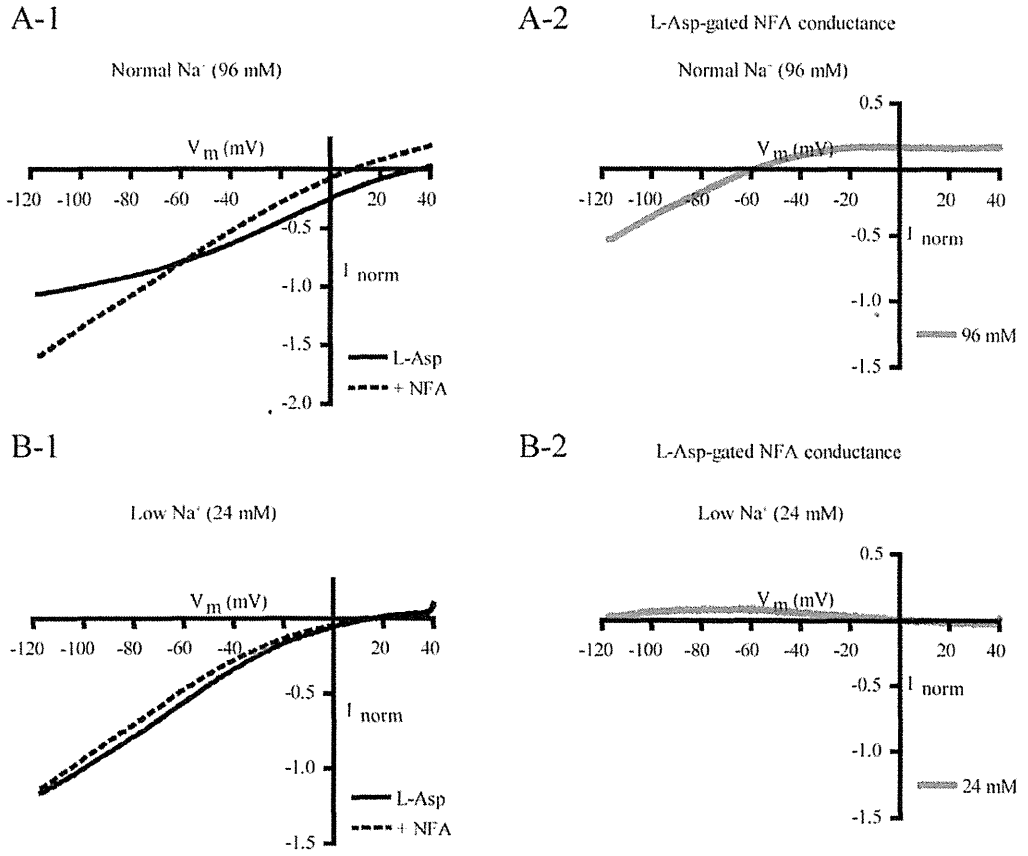

Fig. 4 Influence of Extracellular [Na^+] on L-Asp-Gated NFA-Induced Conductance and the L-Asp Currents in Either the Absence or Presence of NFA

The current–voltage relationships for the L-Asp current in either the absence or presence of NFA were examined under various extracellular [Na^+] by choline substitution. A-1 and B-1: Average current–voltage relationships for L-Asp (30 μM) in either the absence (solid line) or presence (dotted line) of NFA (300 μM) at normal [Na^+] (96 mM) (A-1) and low [Na^+] (24 mM) (B-1). A-2 and B-2: Average current–voltage relationships for the L-Asp-gated NFA-induced conductance at normal [Na^+] (96 mM) (A-2) and low [Na^+] (24 mM) (B-2). The average shift of the sub-E_{rev} gated by L-Asp was -1.1 ± 12.4 mV (n=3) per 10-fold change in [Na^+]. Each point represents the mean from 3 oocytes.

were observed at low [Na^+], suggesting that the modulation of L-Asp currents by NFA depends on the extracellular Na^+ concentration. Comparing the sub-E_{rev} at normal [Na^+] (96 mM) with that at middle-low [Na^+] (48 mM), the average shift of the sub-E_{rev} gated by L-Asp was -1.1 ± 12.4 mV (n=3) per 10-fold change in [Na^+]. In the case of L-Glu, decreasing the extracellular [Na^+] also resulted in a loss of crossover between -120 mV and $+40$ mV (Figs. 5A-1, B-1). The sub-E_{rev} gated by L-Glu was -68 mV at normal [Na^+], whereas no significant subtracted currents were observed at low [Na^+] (Figs. 5A-2, B-2), suggesting that the voltage-dependent modulation of L-Glu currents by NFA depends on the extracellular Na^+ concentration. Comparing the sub-E_{rev} at normal [Na^+] with that at middle-low [Na^+], the average shift of the sub-E_{rev} gated by L-Glu was 7.8 ± 2.2 mV (n=3) per 10-fold change in [Na^+]. This value was not significantly different from that for L-Asp (Student's t-test, p=0.5).

Involvement of Additional Cl^- Conductance Finally, we examined the contribution of additional Cl^- conductance. The current–voltage relationships for the L-Asp current in either the absence or presence of NFA were examined under various extracellular [Cl^-] by gluconate substitution. Figures 6A-1 and B-1 show the average current–voltage relationships for L-Asp in either the absence (solid line) or presence (dotted line) of NFA (300 μM) at normal [Cl^-] (103 mM) (Fig. 6A-1) and low [Cl^-] (30 mM) (Fig. 6B-1). At low [Cl^-], the crossover potential shifted toward the more negative potential (from -61 mV to -115 mV) and the sub-E_{rev} also shifted toward the more negative membrane potential. The average shift of the sub-E_{rev} gated by L-Asp was 94.9 ± 6.7 mV per 10-fold change in [Cl^-] (n=4) (Fig. 6C), indicating that Cl^- contributes to the L-Asp-gated NFA-induced conductance. Regarding L-Glu currents, no changes were observed in the crossover potential at low [Cl^-] (Figs. 7A-1, B-1) and a small shift of the sub-E_{rev} gated by L-Glu occurred at low [Cl^-] (Figs. 7A-2, B-2). The average shift of the sub-E_{rev} gated by L-Glu was 1.9 ± 8.1 mV per 10-fold change in [Cl^-] (n=4) (Fig. 7C), indicating that little contribution of Cl^- to the L-Glu-gated NFA-induced conductance. The significant difference in the additional Cl^- conductance between the L-Asp current and L-Glu current (Student's t-test, $p<0.05$) suggests that mechanisms for the modulation of EAAT1 currents by NFA is substrate-dependent.

DISCUSSION

In this study, we observed that the additional conductances

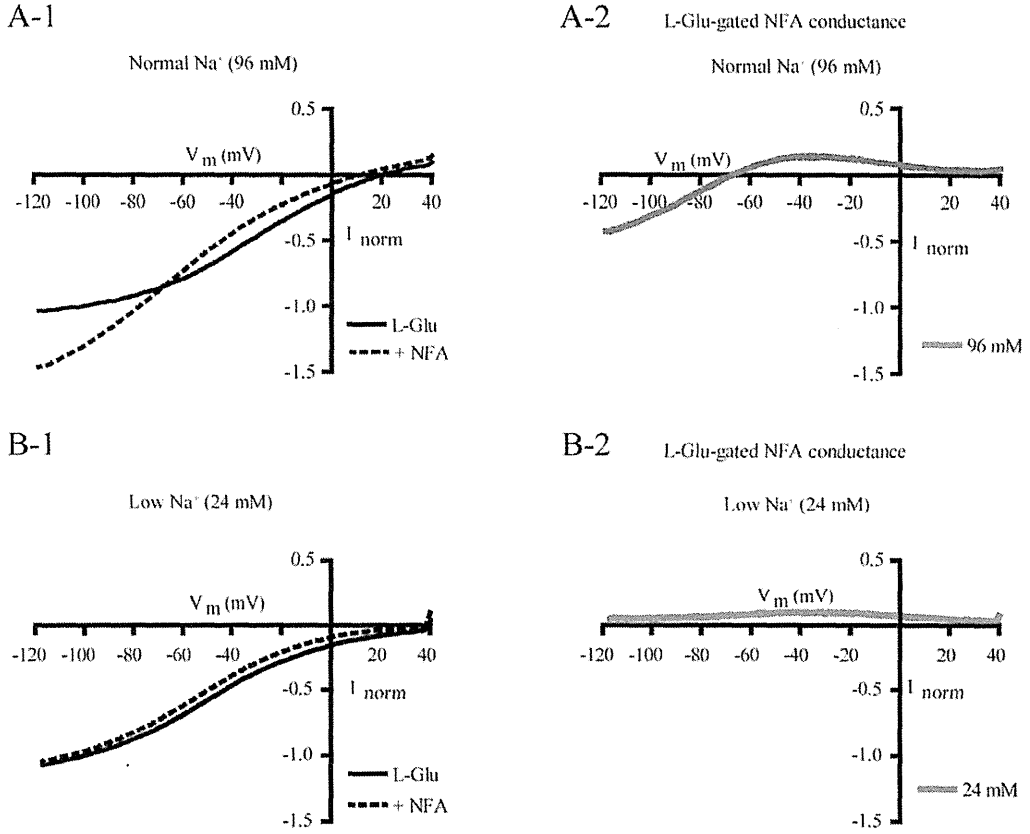

Fig. 5. Influence of Extracellular [Na^+] on L-Glu-Gated NFA-Induced Conductance and the L-Glu Currents in Either the Absence or Presence of NFA

A-1 and B-1: Average current–voltage relationships for L-Glu (30 μM) in either the absence (solid line) or presence (dotted line) of NFA (300 μM) at normal [Na^+] (96 mM) (A-1) and low [Na^+] (24 mM) (B-1). A-2 and B-2: Average current–voltage relationships for the L-Glu-gated NFA-induced conductance at normal [Na^+] (96 mM) (A-2) and low [Na^+] (24 mM) (B-2). The average shift of the sub-E_{rev} gated by L-Glu was 7.8±2.2 mV (n=3) per 10-fold change in [Na^+], which was statistically insignificant compared with that by L-Asp. Each point represents the mean from 5 oocytes.

of EAAT1 were activated when substrates were transported in the presence of NFA. Furthermore, the ionic contribution to the additional conductances is substrate dependent. To our knowledge, this is the first report showing the existence of additional conductances of EAAT1.

Poulsen and Vandenberg reported that NFA induced additional H^+ and Cl^- conductances in *Xenopus* oocytes expressing EAAT4, and these conductances were not thermodynamically coupled to the transport of substrates.[18] These conductances have been referred to as 'slippage.'[24] In our experiments using cultured astrocytes,[25] 300 μM of NFA significantly decreased the L-Glu uptake in cultured astrocytes (data not shown). Membrane potential of cultured astrocytes is approximately −74 mV.[26] Because the crossover potential of the L-Glu currents and NFA (300 μM)-gated L-Glu currents was −72.7±4.5 mV (n=12) in the present study, it is suggested that NFA-gated conductance observed here is not thermodynamically coupled to substrate transport, *i.e.*, NFA induces EAAT1 slippage as well. Transport experiments in voltage-clamped oocytes are necessary to confirm whether additional conductances in EAAT1 are not thermodynamically coupled to the substrate transport.

Sacher *et al.* presented a 'clutch' mechanism for slippage *via* the mammalian and yeast metal-ion transporter DCT1.[27] This mechanism could be explained in terms of two unique but interconnected ion pathways, one dominated by the ion utilized for driving the transport and the other by the transported metal ions. Loose coupling (namely clutching) between the driving force pathway and the metal ion transport pathway generates this observed slippage. Regarding EAAT1, in the presence of NFA, additional H^+ conductance may have arisen as a consequence of a subtle disruption to the ion binding sites, which compromises the coupling between the substrate transport pathway and the ion co-transport ($Na^+/H^+/K^+$) pathway. In support of this, a chimeric transporter generated with EAAT1 and EAAT2, whose junction site is in helical hairpin 2 and in close proximity to the substrate and Na^+ binding site, allows both Na^+ and K^+ to pass through the transporter in the absence of L-Glu.[28]

Interestingly, the ionic contribution is substrate-dependent, *i.e.*, the activation of additional H^+ conductance was involved in the modulation by NFA of both of L-Glu currents and L-Asp currents, whereas Cl^- was only involved in the modulation of L-Asp currents. Wadiche *et al.* reported that Cl^- permeation properties of EAAT1 were substrate-dependent, *i.e.*, the uncoupled Cl^- conductance per transport cycle gated by D-Asp was greater than that gated by L-Glu.[29] The mechanisms underlying the difference between L-Glu and L-Asp observed here may be related the one that causes the greater Cl^- by D-Asp. To elucidate the mechanisms, it is necessary to identify

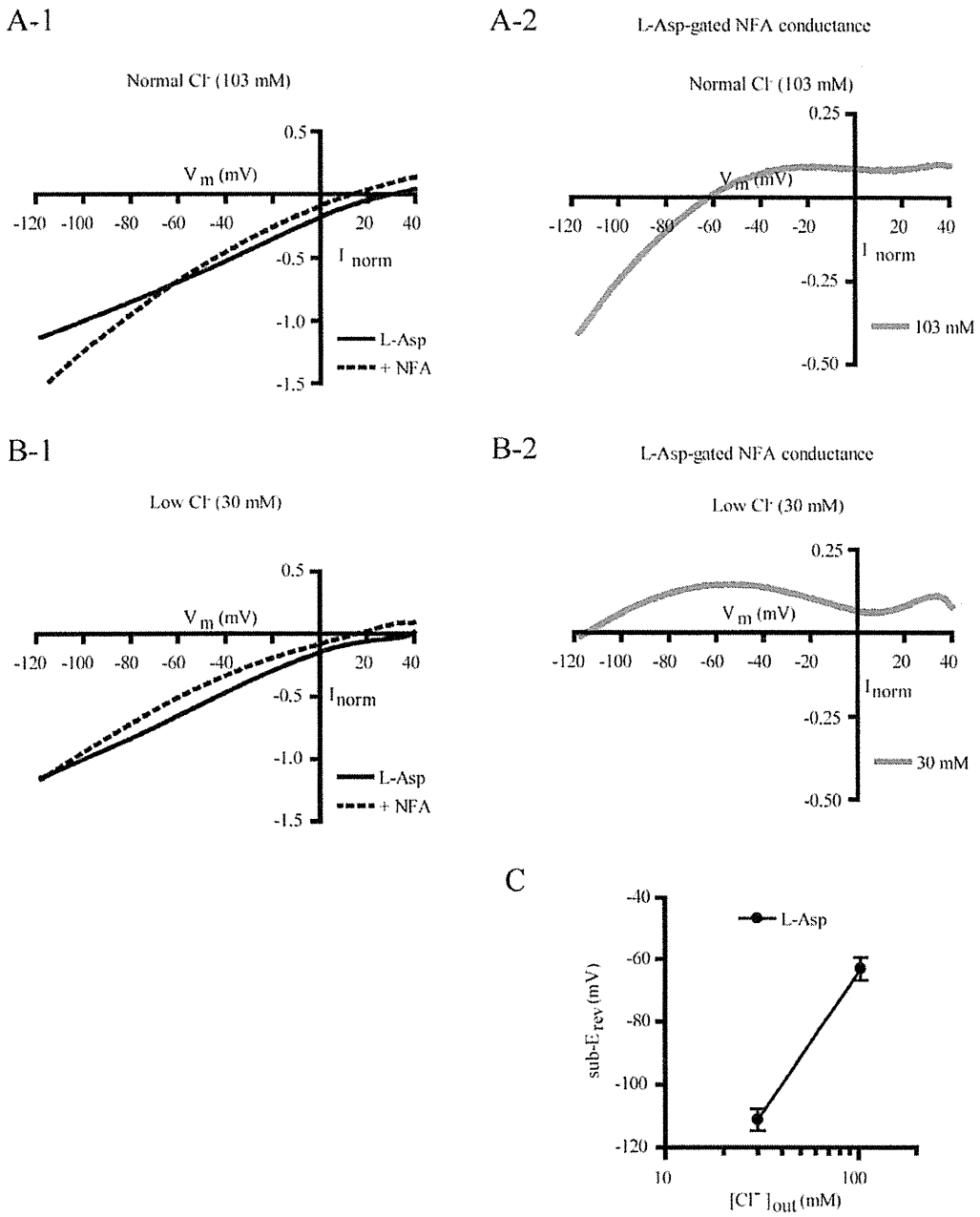

Fig. 6. Influence of Extracellular [Cl^-] on L-Asp-Gated NFA-Induced Conductance and the L-Asp Currents in Either the Absence or Presence of NFA

The current–voltage relationships for the L-Asp current in either the absence or presence of NFA were examined under various extracellular [Cl^-] by gluconate substitution. A-1 and B-1: Average current–voltage relationships for L-Asp (30 μM) in either the absence (solid line) or presence (dotted line) of NFA (300 μM) at normal [Cl^-] (103 mM) (A-1) and low [Cl^-] (30 mM) (B-1). A-2 and B-2: Average current–voltage relationships for the L-Asp-gated NFA-induced conductance at normal [Cl^-] (103 mM) (A-2) and low [Cl^-] (30 mM) (B-2). Each point represents the mean from 5 oocytes. C: Each point (filled circle) represents the mean sub-E_{rev} for L-Asp obtained in A-2 and B-2. Alterations in the extracellular Cl^- concentration caused average shifts of 94.9±6.7 mV per 10-fold change in [Cl^-] (n=4) in the sub-E_{rev}.

the binding site of NFA on EAAT1, and the stoichiometric interaction among the substrates, EAAT1, and NFA.

Alterations in the glial intracellular pH can induce a variety of changes in cellular function, *e.g.*, ionic currents, gap junction conductance, and enzymatic activities.[30] For example, in Bergmann glial cells, which highly express EAAT1,[19,20] electrical coupling *via* gap junctions has been shown to be modulated by altering intracellular pH.[31] Activation of additional H^+ conductance by NFA could be related to the effects of the drug in altering intracellular pH.

In conclusion, we observed substrate-dependent mechanisms for the modulation of EAAT1 currents by NFA. Activation of additional H^+ conductance was involved in the NFA-induced modulation of EAAT1 currents induced by L-Asp and L-Glu. The Cl^- ion was only involved in the NFA-induced modulation of L-Asp currents.

Acknowledgments We would like to thank Dr. Y. Yasu-

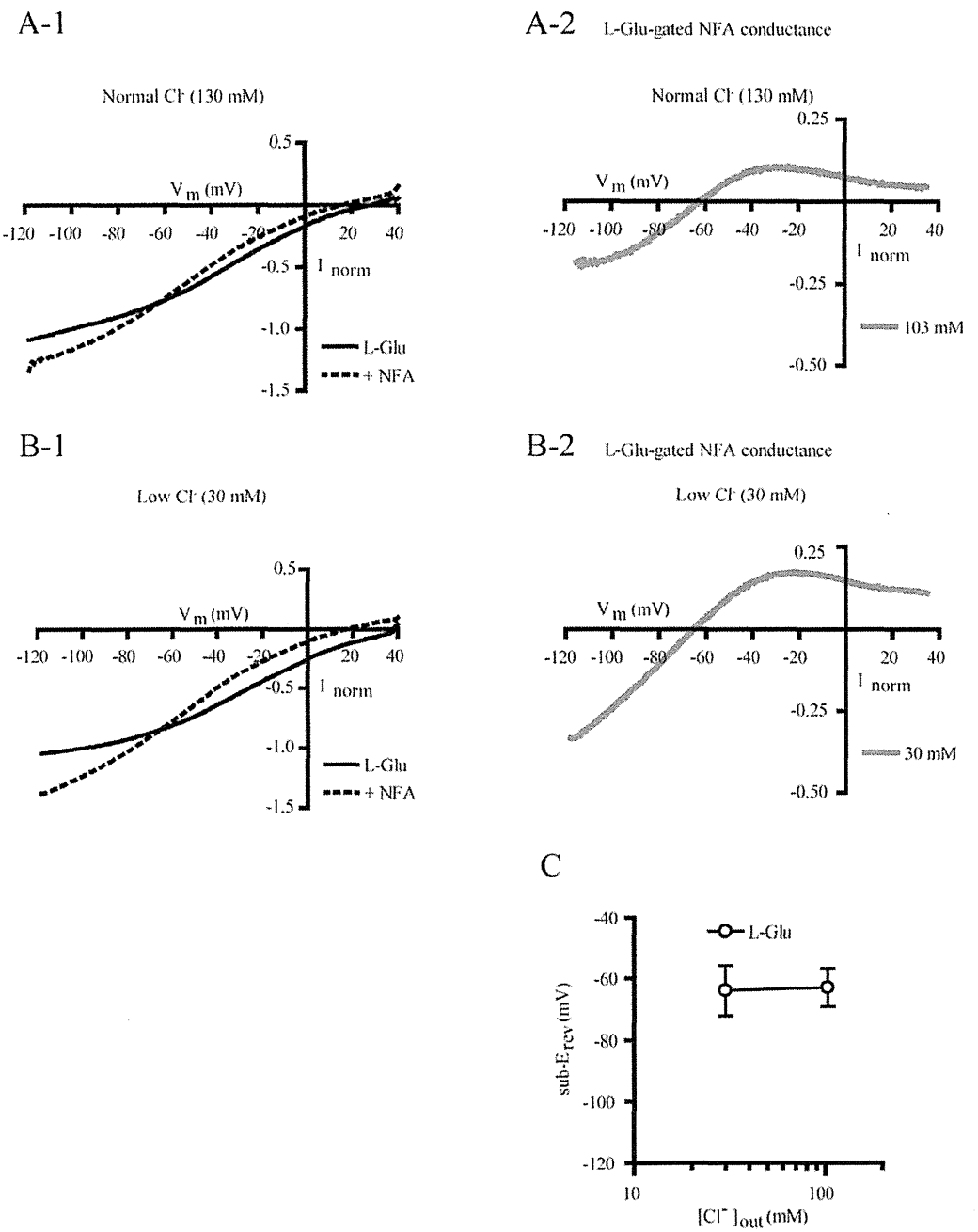

Fig. 7. Influence of Extracellular Cl^- on L-Glu-Gated NFA-Induced Conductance and the L-Glu Currents in Either the Absence or Presence of NFA

A-1 and B-1: Average current–voltage relationships for L-Glu (30 μM) in either the absence (solid line) or presence (dotted line) of NFA (300 μM) at normal [Cl^-] (103 mM) (A-1) and low [Cl^-] (30 mM) (B-1). A-2 and B-2: Average current–voltage relationships for the L-Glu-gated NFA-induced conductance at normal [Cl^-] (103 mM) (A-2) and low [Cl^-] (30 mM) (B-2). Each point represents the mean from 4 oocytes. C: Each point (open circle) represents the mean sub-E_{rev} for L-Glu obtained in A-2 and B-2. Alterations in the extracellular Cl^- concentrations caused average shifts of 1.9±8.1 mV per 10-fold change in [Cl^-] (n=4) in the sub-E_{rev}, which is significantly different from that of L-Asp (Student's t-test, $p<0.05$).

da-Kamatani and Dr. K. Shimamoto for providing the cDNA of EAAT1. We also thank Dr. T. Nakagawa and Dr. Y. Shigeri for their helpful suggestions. This work was partially supported by Grants-in-Aid for Young Scientists from the Ministry of Education, Culture, Sports, Science and Technology of Japan (KAKENHI 18700373, 21700422); Grant-in-Aid from the Food Safety Commission of Japan (No. 1003); the Program for the Promotion of Fundamental Studies in Health Sciences of NIBIO, Japan; a Health and Labour Science Research Grant for Research on Risks of Chemicals; and a Health and Labour Science Research Grant for Research on New Drug Development from MHLW, Japan; a Health and Labour Science Research Grant for Research on Risks of Chemicals from the MHLW, Japan; awarded to K.S. and a Health and Labour Science Research Grant for Research on New Drug Development from MHLW, Japan awarded to Y.S.

REFERENCES

1) Logan WJ, Snyder SH. Unique high affinity uptake systems for glycine, glutamic and aspartic acids in central nervous tissue of the rat. *Nature*, **234**, 297–299 (1971).
2) Zerangue N, Kavanaugh MP. Flux coupling in a neuronal glutamate transporter. *Nature*, **383**, 634–637 (1996).
3) Fairman WA, Vandenberg RJ, Arriza JL, Kavanaugh MP, Amara SG. An excitatory amino-acid transporter with properties of a ligand-gated chloride channel. *Nature*, **375**, 599–603 (1995).
4) Voutsinos-Porche B, Bonvento G, Tanaka K, Steiner P, Welker E, Chatton JY, Magistretti PJ, Pellerin L. Glial glutamate transporters mediate a functional metabolic crosstalk between neurons and astrocytes in the mouse developing cortex. *Neuron*, **37**, 275–286 (2003).
5) Veruki ML, Morkve SH, Hartveit E. Activation of a presynaptic glutamate transporter regulates synaptic transmission through electrical signaling. *Nat. Neurosci.*, **9**, 1388–1396 (2006).
6) Wersinger E, Schwab Y, Sahel JA, Rendon A, Pow DV, Picaud S, Roux MJ. The glutamate transporter EAAT5 works as a presynaptic receptor in mouse rod bipolar cells. *J. Physiol.*, **577**, 221–234 (2006).
7) White MM, Aylwin M. Niflumic and flufenamic acids are potent reversible blockers of Ca^{2+}-activated Cl^- channels in *Xenopus* oocytes. *Mol. Pharmacol.*, **37**, 720–724 (1990).
8) Scott-Ward TS, Li H, Schmidt A, Cai Z, Sheppard DN. Direct block of the cystic fibrosis transmembrane conductance regulator Cl^- channel by niflumic acid. *Mol. Membr. Biol.*, **21**, 27–38 (2004).
9) Ottolia M, Toro L. Potentiation of large conductance KCa channels by niflumic, flufenamic, and mefenamic acids. *Biophys. J.*, **67**, 2272–2279 (1994).
10) Busch AE, Herzer T, Wagner CA, Schmidt F, Raber G, Waldegger S, Lang F. Positive regulation by chloride channel blockers of IsK channels expressed in *Xenopus* oocytes. *Mol. Pharmacol.*, **46**, 750–753 (1994).
11) Wang HS, Dixon JE, McKinnon D. Unexpected and differential effects of Cl^- channel blockers on the Kv4.3 and Kv4.2 K^+ channels. Implications for the study of the I(to2) current. *Circ. Res.*, **81**, 711–718 (1997).
12) Malykhina AP, Shoeb F, Akbarali HI. Fenamate-induced enhancement of heterologously expressed HERG currents in *Xenopus* oocytes. *Eur. J. Pharmacol.*, **452**, 269–277 (2002).
13) Peretz A, Degani N, Nachman R, Uziyel Y, Gibor G, Shabat D, Attali B. Meclofenamic acid and diclofenac, novel templates of KCNQ2/Q3 potassium channel openers, depress cortical neuron activity and exhibit anticonvulsant properties. *Mol. Pharmacol.*, **67**, 1053–1066 (2005).
14) Fernandez D, Sargent J, Sachse FB, Sanguinetti MC. Structural basis for ether-a-go-go-related gene K^+ channel subtype-dependent activation by niflumic acid. *Mol. Pharmacol.*, **73**, 1159–1167 (2008).
15) Zwart R, Oortgiesen M, Vijverberg HP. Differential modulation of alpha 3 beta 2 and alpha 3 beta 4 neuronal nicotinic receptors expressed in *Xenopus* oocytes by flufenamic acid and niflumic acid. *J. Neurosci.*, **15**, 2168–2178 (1995).
16) Hu H, Tian J, Zhu Y, Wang C, Xiao R, Herz JM, Wood JD, Zhu MX. Activation of TRPA1 channels by fenamate nonsteroidal anti-inflammatory drugs. *Pflugers Arch.*, **459**, 579–592 (2010).
17) Furuta A, Rothstein JD, Martin LJ. Glutamate transporter protein subtypes are expressed differentially during rat CNS development. *J. Neurosci.*, **17**, 8363–8375 (1997).
18) Poulsen MV, Vandenberg RJ. Niflumic acid modulates uncoupled substrate-gated conductances in the human glutamate transporter EAAT4. *J. Physiol.*, **534**, 159–167 (2001).
19) Arriza JL, Fairman WA, Wadiche JI, Murdoch GH, Kavanaugh MP, Amara SG. Functional comparisons of three glutamate transporter subtypes cloned from human motor cortex. *J. Neurosci.*, **14**, 5559–5569 (1994).
20) Chaudhry FA, Lehre KP, van Lookeren Campagne M, Ottersen OP, Danbolt NC, Storm-Mathisen J. Glutamate transporters in glial plasma membranes: highly differentiated localizations revealed by quantitative ultrastructural immunocytochemistry. *Neuron*, **15**, 711–720 (1995).
21) Takahashi K, Ishii-Nozawa R, Takeuchi K, Nakazawa K, Sato K. Two non-steroidal anti-inflammatory drugs, niflumic acid and diclofenac, inhibit the human glutamate transporter EAAT1 through different mechanisms. *J. Pharmacol. Sci.*, **112**, 113–117 (2010).
22) DeCoursey TE, Cherny VV. Voltage-activated hydrogen ion currents. *J. Membr. Biol.*, **141**, 203–223 (1994).
23) Fairman WA, Sonders MS, Murdoch GH, Amara SG. Arachidonic acid elicits a substrate-gated proton current associated with the glutamate transporter EAAT4. *Nat. Neurosci.*, **1**, 105–113 (1998).
24) Vandenberg RJ, Huang S, Ryan RM. Slips, leaks and channels in glutamate transporters. *Channels* (Austin), **2**, 51–58 (2008).
25) Sato K, Matsuki N, Ohno Y, Nakazawa K. Estrogens inhibit L-glutamate uptake activity of astrocytes *via* membrane estrogen receptor alpha. *J. Neurochem.*, **86**, 1498–1505 (2003).
26) Nowak L, Ascher P, Berwald-Netter Y. Ionic channels in mouse astrocytes in culture. *J. Neurosci.*, **7**, 101–109 (1987).
27) Sacher A, Cohen A, Nelson N. Properties of the mammalian and yeast metal-ion transporters DCT1 and Smf1p expressed in *Xenopus laevis* oocytes. *J. Exp. Biol.*, **204**, 1053–1061 (2001).
28) Vandenberg RJ, Arriza JL, Amara SG, Kavanaugh MP. Constitutive ion fluxes and substrate binding domains of human glutamate transporters. *J. Biol. Chem.*, **270**, 17668–17671 (1995).
29) Wadiche JI, Amara SG, Kavanaugh MP. Ion fluxes associated with excitatory amino acid transport. *Neuron*, **15**, 721–728 (1995).
30) Deitmer JW, Rose CR. pH regulation and proton signalling by glial cells. *Prog. Neurobiol.*, **48**, 73–103 (1996).
31) Muller T, Moller T, Neuhaus J, Kettenmann H. Electrical coupling among Bergmann glial cells and its modulation by glutamate receptor activation. *Glia*, **17**, 274–284 (1996).

Journal of Pharmacological Sciences xxx (2014) 1–5

Contents lists available at ScienceDirect

Journal of Pharmacological Sciences

journal homepage: www.elsevier.com/locate/jphs

Short communication

Paroxetine prevented the down-regulation of astrocytic L-Glu transporters in neuroinflammation

Koki Fujimori [a, b], Junpei Takaki [a, b], Yukari Shigemoto-Mogami [a], Yuko Sekino [a], Takeshi Suzuki [b], Kaoru Sato [a, *]

[a] Laboratory of Neuropharmacology, Division of Pharmacology, National Institute of Health Sciences, 1-18-1 Kamiyoga, Setagaya-ku, Tokyo 158-8501, Japan
[b] Division of Basic Biological Science, Faculty of Pharmacy, Keio University, 1-5-30 Shiba-koen, Minato-ku, Tokyo 105-8512, Japan

ARTICLE INFO

Article history:
Received 4 August 2014
Received in revised form
26 August 2014
Accepted 18 September 2014
Available online xxx

Keywords:
Paroxetine
L-glutamate
Inflammation

ABSTRACT

The extracellular L-glutamate (L-Glu) concentration is elevated in neuroinflammation, thereby causing excitotoxicity. One of the mechanisms is down-regulation of astrocyte L-Glu transporters. Some antidepressants have anti-inflammatory effects. We therefore investigated effects of various antidepressants on the down-regulation of astrocyte L-Glu transporters in the in vitro neuroinflammation model. Among these antidepressants, only paroxetine was effective. We previously demonstrated that the down-regulation of astrocyte L-Glu transporters was caused by L-Glu released from activated microglia. We here clarified that only paroxetine inhibited L-Glu release from microglia. This is the novel action of paroxetine, which may bring advantages on the therapy of neuroinflammation.

Increasing evidence indicates that inflammatory processes play important roles in the pathogenesis of many neurodegenerative disorders (1–3). Under the neuroinflammatory conditions, it is known that the extracellular concentration of L-glutamate (L-Glu) and inflammatory mediators, such as proinflammatory cytokines, prostaglandins, free radicals and complements are elevated (4). L-Glu is one of the most abundant excitatory neurotransmitters in the mammalian CNS. The released L-Glu is immediately uptaken by astrocyte L-Glu transporters, GLAST (EAAT1 in human) and GLT-1 (EAAT2 in human), or sustained elevation of extracellular concentration of L-Glu induce excitotoxicity. The impairment of the astrocyte L-Glu transporters is reported in various neurological disorders including Alzheimer's disease (5), Parkinson's diseases (6) and amyotrophic lateral sclerosis (7). We found that the expression level of L-Glu transporters in astrocytes of astrocyte-microglia-neuron mixed culture was decreased in the *in vitro* model of the early stage of inflammation in the previous study (8). We clarified the interaction between astrocytes and microglia underlie the down-regulation of L-Glu transporters, i.e., activated microglia release L-Glu and the resulting elevation of extracellular L-Glu cause down-regulation of astrocytic L-Glu transporters. Some antidepressants are known to have anti-inflammatory effects (9, 10). In this study, therefore, we investigated the effects of various antidepressants on the decrease in the astrocytic L-Glu transporter function in the early stage of inflammation and the contribution of microglia to the effects.

Astrocyte-microglia-neuron mixed culture and microglia culture were performed according to the methods previously described (8). Antidepressants and serotonin (5-HT) were dissolved in PBS at 100 μM and 10 mM, respectively, and were diluted with culture medium at the time of use. At 8 DIV, the astrocyte-microglia-neuron mixed culture was treated with 10 ng/mL LPS for 72 h. Antidepressants were applied from 1 h before to the end of the LPS-treatment. Then the concentration of the L-Glu remaining in the culture medium 30 min after changing extracellular concentration of L-Glu to 100 μM was measured. The measurement of the extracellular L-Glu concentration in the medium was performed according to the methods previously described (8). Real-Time Quantitative RT-PCR, Western blotting, immunocytochemistry were also performed according to the methods previously

Abbreviations: ATP, adenosine 5′-triphosphate; CNS, central nervous system; DIV, days *in vitro*; GABA, γ-aminobutyric acid; L-glu, L-glutamate; LPS, lipopolysaccharide; PBS, phosphate-buffered saline; $P2X_4$, P2X prinoceptor 4; RNA, ribonucleic acid; SD, Sprague-Dawley; SDS, sodium dodecyl sulfate; SNRI, serotonin–norepinephrine reuptake inhibitor; SSRI, selective serotonin reuptake inhibitor; TCA, tricyclic antidepressant; 5-HT, 5-hydroxytryptamine.

* Corresponding author. Tel./fax: +81 3 3700 9698.
E-mail address: kasato@nihs.go.jp (K. Sato).

Peer review under responsibility of Japanese Pharmacological Society.

http://dx.doi.org/10.1016/j.jphs.2014.09.002

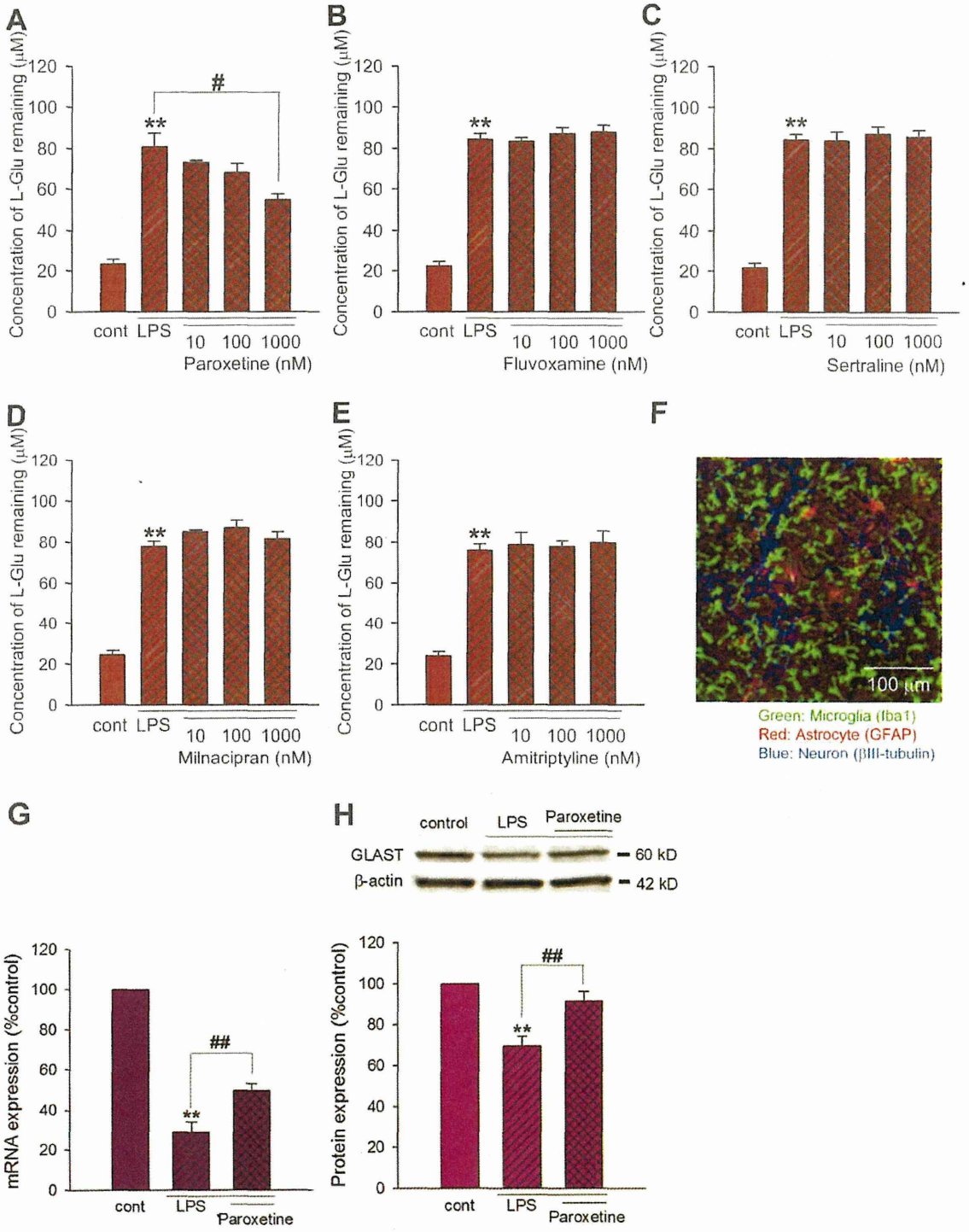

Fig. 1. Effects of antidepressants on the decreased L-Glu transport activity under the inflammatory condition. A–E. Antidepressants were applied to the mixed culture from 1 h before to the end of the LPS-treatment (10 ng/ml, 72 h). L-Glu transport activity was quantified as the L-Glu remaining 30 min after changing the extracellular concentration to 100 μM. Paroxetine prevented the LPS-induced decrease in the L-Glu transport activity in a concentration-dependent manner (A). Fluvoxamine (B), sertraline (C), milnacipran (D), and amitriptyline (E) had no effects. **: $p < 0.01$ vs. control group, #: $p < 0.05$ vs. LPS-treated group, Tukey's test following ANOVA ($N = 6$). F. Typical image of the microglia-astrocyte-neuron mixed culture immunostained with cell type-specific markers (Iba1: microglia; GFAP: astrocytes; βIII tubulin: neurons). G, H. Effects of paroxetine on the expression level of GLAST. Mixed cultures were treated with LPS (10 ng/ml) in the absence or presence of the paroxetine for 24 h (for mRNA level quantification) or 72 h (for protein level quantification). The expression level of GLAST was quantified at mRNA level (G) and protein level (H). LPS (10 ng/ml) caused significant decrease in GLAST mRNA level and paroxetine significantly prevented the decrease (G). LPS (10 ng/ml) caused significant decrease in GLAST protein level and paroxetine almost completely prevented the decrease (H). **: $p < 0.01$ vs. control group, ##: $p < 0.01$ vs. LPS-treated group, Tukey's test following ANOVA ($N = 5$).

Please cite this article in press as: Fujimori K, et al., Paroxetine prevented the down-regulation of astrocytic L-Glu transporters in neuroinflammation, Journal of Pharmacological Sciences (2014), http://dx.doi.org/10.1016/j.jphs.2014.09.002

described (8). The microglia culture was treated with LPS for 24 h in the presence or absence of antidepressants and the concentration of L-Glu in the medium was measured. All sets of the experiments were repeated in triplicate. All procedures described above were in accordance with institutional guidelines.

In the previous report, we showed that the expression level of astrocytic L-Glu transporters was decreased in the astrocyte-microglia-neuron mixed culture in LPS (10 ng/ml, 72 h)-induced inflammation model without cell death (8). We first compared the effects of various groups of antidepressants, i.e., selective serotonin reuptake inhibitors (SSRIs) (paroxetine, fluvoxamine, and sertraline), serotonin–norepinephrine reuptake inhibitor (SNRI) (milnacipran), and tricyclic antidepressant (TCA) (amitriptyline), on the decrease in the astrocytic L-Glu transporter function in this inflammation model. To quantify L-Glu transport activity, we measured the concentration of L-Glu remaining 30 min after changing the medium to the one containing 100 μM of L-Glu. In each set of experiment, LPS-induced decrease in the L-Glu transport activity was stably reproduced (Fig. 1A–E). Among antidepressants, only paroxetine prevented the LPS-induced decrease in L-Glu transport activity (Fig. 1A). The effect was concentration-dependent and reached significant at 1 μM. The other antidepressants had no effects (Fig. 1B–E). Typical image of the astrocyte-microglia-neuron mixed culture was shown in Fig. 1F. We have clarified that LPS-induced decrease in L-Glu transport activity was caused by the decrease in the expression level of GLAST, a predominant L-Glu transporter in the mixed culture, in both of mRNA and protein levels (8). In this study, LPS-induced decreases in the expression of GLAST, were reproduced at both of mRNA (28.8 ± 4.7% of the control) and protein (69.5 ± 4.7% of the control) levels (Fig. 1G, H). We then examined the effects of paroxetine on the LPS-induced decrease in the L-Glu transporter expression. Paroxetine significantly prevented the decreases at both of mRNA (28.8 ± 4.7 to 49.6 ± 3.3%; $n = 10$) and protein (from 69.5 ± 4.7% to 91.0 ± 5.1%; $n = 5$) levels (Fig. 1G, H). As is shown in Fig. 1, fluvoxamine and sertraline, the other SSRIs in this study, did not affect the decrease in L-Glu transport activity, suggesting that paroxetine revealed the effects through the mechanisms independent of its inhibitory effect on serotonin selective transporter. In support of this, LPS-induced decrease in L-Glu transport activity was not changed by the elevation of extracellular serotonin concentration (Fig. 2A). We also confirmed that paroxetine did not directly affect the L-Glu transport activity of the astrocyte culture (Fig. 2B). In our previous report, the down-regulation of GLAST in the inflammation model was caused by the elevation of extracellular L-Glu released from microglia (8). We therefore compared the effects of the antidepressants on LPS-induced L-Glu release from microglia. When microglia culture was treated with 10 ng/ml LPS for 24 h in the presence or absence of the antidepressants, only paroxetine suppressed L-Glu release in a concentration-dependent manner (Fig. 3A). The other antidepressants had no effects (Fig. 3B–E). We confirmed that paroxetine did not affect the microglial viability until 10 μM by LDH assay (data not shown). These results strongly suggest that the protective effect of paroxetine on the LPS-induced down-regulation of astrocytic L-Glu transporters was caused by the suppression of L-Glu release from microglia.

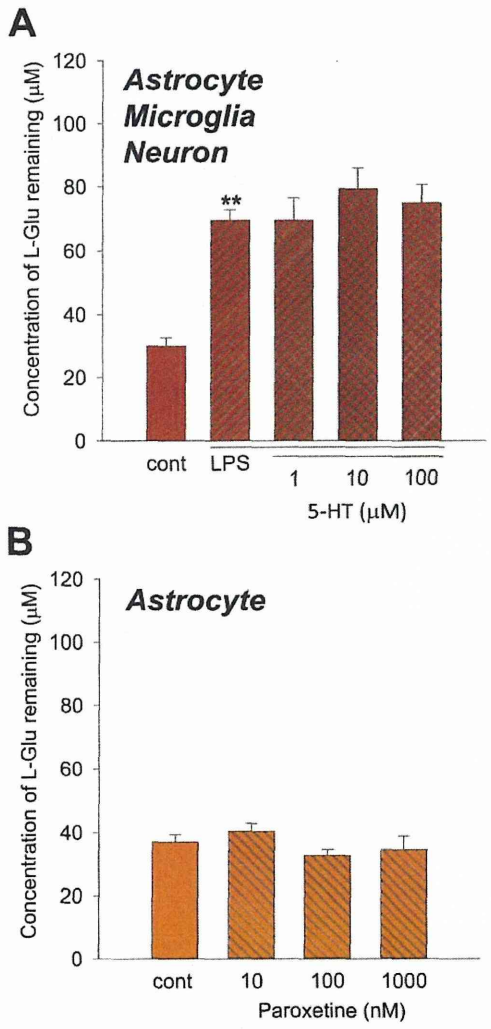

Fig. 2. Relation of the effects of paroxetine on LPS-induced decrease in L-Glu transport activity with its SSRI function and the direct effect on astrocytes. A. 72 h treatment with 5-HT (1–100 μM) did not affect LPS-induced decrease in the L-Glu transport activity. B. 72 h treatment with paroxetine (10–1000 nM) of astrocyte culture did not affect its L-Glu transport activity. **: $p < 0.01$ vs. control group, Tukey's test following ANOVA ($N = 6$).

The shape of microglia in the mixed culture was dramatically changed to amoeboid type by LPS and this morphological change was remarkably suppressed by paroxetine (unpublished observation). This suggests that paroxetine does not only suppress L-Glu release from microglia alone but also microglial activation. To demonstrate this possibility, the effect of paroxetine on the microglial activation is needed to be confirmed using multiple parameters. Because SSRIs have diverse chemical structures despite a common mode of action of 5-HT function (11), it is possible that paroxetine revealed the effects through interaction with paroxetine-specific target molecules. Because paroxetine exhibited the powerful inhibition of calcium influx via $P2X_4$ receptors (12), $P2X_4$ receptor is one of the most probable candidate molecules. The expression level of $P2X_4$ receptor in microglia is up-regulated in inflammatory pain model in spinal cord and is thought to be important for microglial inflammatory responses (13). MAPK signaling molecules (14) and GABA(B) receptor (15) are possibly involved in the paroxetine-specific effects as well. The effective concentration of paroxetine to reduce L-Glu release was 1 μM. According to the attached documents of paroxetine (http://www.info.pmda.go.jp/), intracerebral concentration of paroxetine reaches 77 nM by 25 mg/day-repeated administration. It is therefore unlikely that paroxetine affects astrocyte L-Glu transporters and microglia by the general dosage of SSRI. For clinical application of our present findings, further investigation concerning application period and dosage is needed.

Please cite this article in press as: Fujimori K, et al., Paroxetine prevented the down-regulation of astrocytic L-Glu transporters in neuroinflammation, Journal of Pharmacological Sciences (2014), http://dx.doi.org/10.1016/j.jphs.2014.09.002

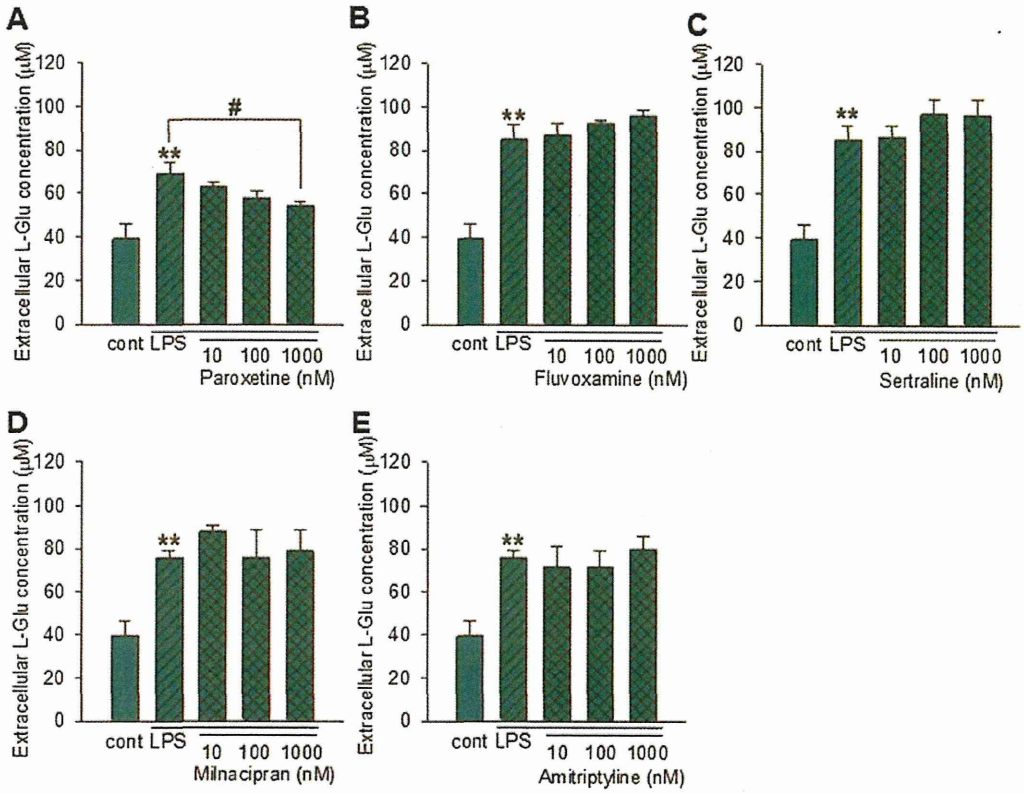

Fig. 3. Effects of antidepressants on the L-Glu release from microglia under the inflammatory condition. In each set of experiment, antidepressants were applied to the mixed culture from 1 h before to the end of the LPS-treatment (10 ng/ml, 24 h). The extracellular concentration of L-Glu was quantified. Paroxetine prevented the LPS-induced L-Glu release from microglia in a concentration-dependent manner (A). Fluvoxamine (B), sertraline (C), milnacipran (D), and amitriptyline (E) had no effects on LPS-induced L-Glu release from microglia. **: $p < 0.01$ vs. control group, #: $p < 0.05$ vs. LPS-treated group, Tukey's test following ANOVA ($N = 6$).

In conclusion, we found that paroxetine inhibit the L-Glu release from activated microglia and prevent down-regulation of astrocytic L-Glu transporters in the early stage of neuroinflammation. This is the novel pharmacological effect of paroxetine, which may bring advantages on the therapy of the disease associated with neuroinflammation.

Conflicts of interest

I declare that I have no significant competing financial, professional or personal interests that might have influenced the results and interpretation of the manuscript.

Author's contributions

K.F. performed experiments and manuscript writing.
J.T. performed experiments.
Y.S-M. provided advice on manuscript writing
Y.S. provided advice on manuscript writing
T.S. provided advice on the experimental direction and manuscript writing.
K.S. designed the experimental plan and performed experiments, manuscript writing.

Acknowledgments

This work was partly supported by a Grant-in-Aid for Young Scientists from Ministry of Education, Culture, Sports, Science, and Technology, Japan (KAKENHI 21700422), the Program for Promotion of Fundamental Studies in Health Sciences of National Institute of Biomedical Innovaton (10-21), Japan, a Health and Labor Science Research Grant for Research on Risks of Chemicals, a Labor Science Research Grant for Research on New Drug Development from the MHLW, Japan, awarded to K.S., Grant-in-Aid for research from MEXT, Japan (KAKENHI C23590113) awarded to T.S., and a Health and Labor Science Research Grant for Research on Publicly Essential Drugs and Medical Devices, Japan, awarded to Y.S.

References

(1) Bowerman M, Vincent T, Scamps F, Perrin FE, Camu W, Raoul C. Neuroimmunity dynamics and the development of therapeutic strategies for amyotrophic lateral sclerosis. Front Cell Neurosci. 2013;7:214.
(2) Limatainen S, Lehtimaki K, Palmio J, Alapirtti T, Peltola J. Immunological perspectives of temporal lobe seizures. J Neuroimmunol. 2013;263:1–7.
(3) Schwartz M, Baruch K. The resolution of neuroinflammation in neurodegeneration: leukocyte recruitment via the choroid plexus. EMBO J. 2014;33:7–22.
(4) Lucas SM, Rothwell NJ, Gibson RM. The role of inflammation in CNS injury and disease. Br J Pharmacol. 2006;147(Suppl. 1):S232–S240.
(5) Mashah E, Alford M, DeTeresa R, Mallory M, Hansen L. Deficient glutamate transport is associated with neurodegeneration in Alzheimer's disease. Ann Neurol. 1996;40:759–766.
(6) Ferrarese C, Zoia C, Pecora N, Piolti R, Frigo M, Bianchi G, et al. Reduced platelet glutamate uptake in Parkinson's disease. J Neural Transm. 1999;106:685–692.
(7) Rothstein JD, Martin LJ, Kuncl RW. Decreased glutamate transport by the brain and spinal cord in amyotrophic lateral sclerosis. N Engl J Med. 1992;326:1464–1468.
(8) Takaki J, Fujimori K, Miura M, Suzuki T, Sekino Y, Sato K. L-glutamate released from activated microglia downregulates astrocytic L-glutamate transporter

Please cite this article in press as: Fujimori K, et al., Paroxetine prevented the down-regulation of astrocytic L-Glu transporters in neuroinflammation, Journal of Pharmacological Sciences (2014), http://dx.doi.org/10.1016/j.jphs.2014.09.002

expression in neuroinflammation: the 'collusion' hypothesis for increased extracellular L-glutamate concentration in neuroinflammation. J Neuroinflammation. 2012;9:275.
(9) Hashioka S, Klegeris A, Monji A, Kato T, Sawada M, McGeer PL, et al. Antidepressants inhibit interferon-gamma-induced microglial production of IL-6 and nitric oxide. Exp Neurol. 2007;206:33–42.
(10) Hwang J, Zheng LT, Ock J, Lee MG, Kim SH, Lee HW, et al. Inhibition of glial inflammatory activation and neurotoxicity by tricyclic antidepressants. Neuropharmacology. 2008;55:826–834.
(11) RJ B. Drugs and the treatment of psychiatric disorders. Goodman and Gilman's the pharmacological basis of therapeutics. In: Hardman JG, Limbird LE, Gilman AG, editors. 10th ed 2001. p. 447–483.
(12) Nagata K, Imai T, Yamashita T, Tsuda M, Tozaki-Saitoh H, Inoue K. Antidepressants inhibit P2X4 receptor function: a possible involvement in neuropathic pain relief. Mol Pain. 2009;5:20.
(13) Guo LH, Trautmann K, Schluesener HJ. Expression of P2X4 receptor by lesional activated microglia during formalin-induced inflammatory pain. J Neuroimmunol. 2005;163:120–127.
(14) Liu RP, Zou M, Wang JY, Zhu JJ, Lai JM, Zhou LL, et al. Paroxetine ameliorates lipopolysaccharide-induced microglia activation via differential regulation of MAPK signaling. J Neuroinflammation. 2014;11:47.
(15) Khundakar AA, Zetterstrom TS. Effects of GABAB ligands alone and in combination with paroxetine on hippocampal BDNF gene expression. Eur J Pharmacol. 2011;671:33–38.

Please cite this article in press as: Fujimori K, et al., Paroxetine prevented the down-regulation of astrocytic L-Glu transporters in neuroinflammation, Journal of Pharmacological Sciences (2014), http://dx.doi.org/10.1016/j.jphs.2014.09.002

Development/Plasticity/Repair

Microglia Enhance Neurogenesis and Oligodendrogenesis in the Early Postnatal Subventricular Zone

Yukari Shigemoto-Mogami,[1] Kazue Hoshikawa,[1] James E. Goldman,[2] Yuko Sekino,[1] and Kaoru Sato[1]

[1]Laboratory of Neuropharmacology, Division of Pharmacology, National Institute of Health Sciences, Tokyo 158-8501, Japan, and [2]Department of Pathology and Cell Biology, Columbia University College of Physicians and Surgeons, New York, New York 10032

Although microglia have long been considered as brain resident immune cells, increasing evidence suggests that they also have physiological roles in the development of the normal CNS. In this study, we found large numbers of activated microglia in the forebrain subventricular zone (SVZ) of the rat from P1 to P10. Pharmacological suppression of the activation, which produces a decrease in levels of a number of proinflammatory cytokines (i.e., IL-1β, IL-6, TNF-α, and IFN-γ) significantly inhibited neurogenesis and oligodendrogenesis in the SVZ. *In vitro* neurosphere assays reproduced the enhancement of neurogenesis and oligodendrogenesis by activated microglia and showed that the cytokines revealed the effects complementarily. These results suggest that activated microglia accumulate in the early postnatal SVZ and that they enhance neurogenesis and oligodendrogenesis via released cytokines.

Key words: cytokine; microglia; neurogenesis; neurosphere; oligodendrogenesis; subventricular zone

Introduction

CNS microglia have long been considered as resident immune cells, which are activated in response to pathological events. In pathological conditions, they change their morphology to an amoeboid shape, acquiring activation-specific phenotypes, such as chemotaxis, phagocytosis, and secretion of inflammatory cytokines (Nakajima and Kohsaka, 2001; Inoue, 2008; Monji et al., 2009; Kettenmann et al., 2011). However, microglia also have physiological roles in the normal CNS. They actively survey their territory with fine processes and receive stimuli from the environment as sensor cells (Kettenmann et al., 2011). *In vivo* lineage tracing studies have established that microglia differentiate from primitive myeloid progenitors that arise before embryonic day 8 and are identified in the CNS parenchyma even before definitive hematopoiesis (Ginhoux et al., 2010), whereas it has also been shown that microglia migrate from the lateral ventricle into the brain via the subventricular zone (SVZ) in the postnatal brain (Mohri et al., 2003). In the early embryonic brain, most microglia adopt an amoeboid morphology and characteristics of an activated form (Hirasawa et al., 2005). Microglia in the embryonic SVZ limit the production of cortical neurons by phagocytosing neural precursor cells (Cunningham et al., 2013). The number of microglia in the brain reaches a maximum during the early postnatal weeks (Wu et al., 1993; Xu and Ling, 1994), after which they transform into cells with a ramified shape, the typical morphology observed in the adult CNS (Ignácio et al., 2005). However, microglia are densely populated in neurogenic niches, such as the SVZ (Mosher et al., 2012), and appear more activated in the adult SVZ than in non-neurogenic zones (Goings et al., 2006). These developmental changes in the activation and the distribution of microglia strongly suggest that microglia play important roles in CNS development. However, the developmental dynamics of microglia in the postnatal SVZ and their roles in neurogenesis and gliogenesis at this stage are not well understood. We have examined the distribution and morphology of microglia in the rat forebrain during the neonatal-early postnatal period in detail and found a large number of active forms within the SVZ from P1 to P10, which then transformed from an activated form to a ramified form after P14. We here present evidence that microglia in the early postnatal SVZ promote both neurogenesis and oligodendrogenesis and that cytokines are important in these effects. To our knowledge, this is the first report showing a novel physiological function of microglia regulating neurogenesis and oligodendrogenesis in the early postnatal brain.

Materials and Methods

Animals and treatment. All animals were treated in accordance with the guidelines for the Care and Use of Laboratory Animals of the Animal Research Committee of the National Institute of Health Sciences and followed the *Guide for the Care and Use of Laboratory Animals*. All experiments were approved by the Animal Research Committee of National Institute of Health Sciences and conformed to the relevant regulatory standards. The Wistar rats were purchased from Japan SLC and maintained under specific pathogen-free conditions at a controlled temperature and humidity and on a 12 h light/12 h dark cycle and had *ad libitum*

Received April 15, 2013; revised Dec. 21, 2013; accepted Dec. 27, 2013.

Author contributions: K.S. designed research; Y.S.-M., K.H., and K.S. performed research; Y.S.-M., K.H., J.E.G., Y.S., and K.S. analyzed data; Y.S.-M., J.E.G., Y.S., and K.S. wrote the paper.

This work was supported in part by a Grant-in-Aid for Young Scientists from MEXT, Japan (KAKENHI 21700422), the Program for Promotion of Fundamental Studies in Health Sciences of NIBIO, Japan, a Health and Labor Science Research Grant for Research on Risks of Chemicals, a Labor Science Research Grant for Research on New Drug Development from the MHLW, Japan to K.S., and a Health and Labor Science Research Grant for Research on Publicly Essential Drugs and Medical Devices, Japan to Y.S.

The authors declare no competing financial interests.

This article is freely available online through the *J Neurosci* Author Open Choice option.

Correspondence should be addressed to Dr. Kaoru Sato, Laboratory of Neuropharmacology, Division of Pharmacology, National Institute of Health Sciences, Kamiyoga 1-18-1, Setagaya-ku, Tokyo 158-8501, Japan. E-mail: kasato@nihs.go.jp.

DOI:10.1523/JNEUROSCI.1619-13.2014

 0270-6474/14/342231-13$15.00/0